ChemComm

COMMUNICATION

View Article Online
View Journal | View Issue

Cite this: *Chem. Commun.*, 2018, **54**, 10100

Received 3rd August 2018,
Accepted 13th August 2018

DOI: 10.1039/c8cc06331a

rsc.li/chemcomm

Enhanced electrocatalysis for alkaline hydrogen evolution by Mn doping in a Ni_3S_2 nanosheet array†

Huitong Du,[a] Rongmei Kong,[a] Fengli Qu*[a] and Limin Lu*[b]

Developing earth-abundant and efficient catalysts for the hydrogen evolution reaction (HER) is highly desirable. In this communication, we report the development of a Mn-doped Ni_3S_2 nanosheet array on Ni foam (Mn-Ni_3S_2/NF) as a superior and durable catalyst for alkaline hydrogen evolution. Such Mn-Ni_3S_2/NF demands an overpotential of 152 mV to afford 10 mA cm^{-2} in 1.0 M KOH, 46 mV less than that for Ni_3S_2/NF. Furthermore, this catalyst also shows high long-term electrochemical durability. This work provides important guidance for exploring optimal HER catalysts.

The increasing fossil fuel crisis and accompanying environmental pollution have boosted an urgent demand for clean and renewable energy.[1,2] Hydrogen, as a sustainable clean energy source, is a promising alternative to traditional fossil fuels.[3] Water electrolysis offers an attractive route to produce pure hydrogen,[4] but its large-scale application is hindered by the sluggish kinetics of the hydrogen evolution reaction (HER).[5] Thus, high-performance HER catalysts are required to drive high current density at low overpotentials.[6,7] Currently, platinum (Pt) is considered to be the best HER catalyst, but the limited storage and high cost hinder its widespread use.[8] Hence, it is highly desirable to develop earth-abundant catalysts with efficient performance for hydrogen evolution.

Nickel has emerged as an attractive non-noble metal element for hydrogen evolution with high catalytic activity in recent years.[9–12] Transition metal sulfides, such as ultrathin CoS_2 shells,[13] $NiS_{1.03}$[14] and NiS_2,[15] have received increasing attention for applications in catalysis because of their excellent performance and high conductivity. Among these compounds, Ni_3S_2 stood out because of its low cost and facile fabrication processes.[16–18] In order to further improve its catalytic performance for the alkaline HER, metallic element doping has been proposed as an effective strategy to make Ni_3S_2 splitting of water more energy-efficient by virtue of its increased catalytic sites, enhanced electronic conductivity and optimized hydrogen adsorption energy.[19–24] Mn-based compounds are considered as outstanding catalysts for water oxidization, meanwhile, the rich reserve and low price of Mn element make it a promising dopant.[25,26] Therefore, we anticipate that Mn doping in Ni_3S_2 would greatly promote the electrocatalytic HER performance under alkaline conditions.

In this communication, we report the synthesis of a Mn-doped Ni_3S_2 nanosheet array grown on Ni foam (Mn-Ni_3S_2/NF) as an efficient catalyst for the HER with good durability in alkaline media. Such Mn-Ni_3S_2/NF achieves a low overpotential of 152 mV at 10 mA cm^{-2} in 1.0 M KOH, 46 mV less than that of Ni_3S_2/NF. In addition, this catalyst also presents good long-term electrochemical durability with the maintenance of its catalytic activity for at least 20 h.

Mn-Ni_3S_2/NF was derived from its hydroxide precursor through a facile hydrothermal sulfide reaction (see the ESI† for preparation details). Fig. 1a shows the X-ray powder diffraction (XRD) pattern of Mn-Ni_3S_2/NF. The diffraction peaks at 21.7°, 31.1°, 37.8°, 44.3°, 49.7°, 50.1°, 55.1° and 55.3° can be indexed to the (101), (110), (003), (202), (113), (211), (122) and (300) planes of Ni_3S_2 (JCPDS No. 44-1418), respectively. The other peaks correspond to NF. Interestingly, no other Mn-based diffraction peaks are observed in the XRD pattern of Mn-Ni_3S_2/NF compared with pure Ni_3S_2 (Fig. S1, ESI†), suggesting that Mn atoms should be stabilized in a doping state in the atomic structure of Ni_3S_2.[27,28] Inductively coupled plasma mass spectrometry (ICP-MS) analysis suggests the presence of Mn, Ni and S with an atomic ratio of 0.05 : 0.65 : 0.30. The scanning electron microscopy (SEM) image of the hydroxide precursor (Fig. 1b) shows that the nanosheet array uniformly grows on the bare NF (Fig. S2, ESI†). After the hydrothermal sulfide reaction, the SEM image indicates that the sulfided product still maintains the nanosheet nature but becomes rough (Fig. 1c). The transmission electron microscopy (TEM) image of the resulting Mn-Ni_3S_2 further confirms its

[a] College of Chemistry and Chemical Engineering, Qufu Normal University, Qufu 273165, Shandong, China. E-mail: fengliquhn@hotmail.com
[b] Institute of Functional Materials and Agricultural Applied Chemistry, College of Science, Jiangxi Agricultural University, Nanchang 330045, P. R. China. E-mail: lulimin816@hotmail.com

† Electronic supplementary information (ESI) available: Experimental section and supplementary figures. See DOI: 10.1039/c8cc06331a

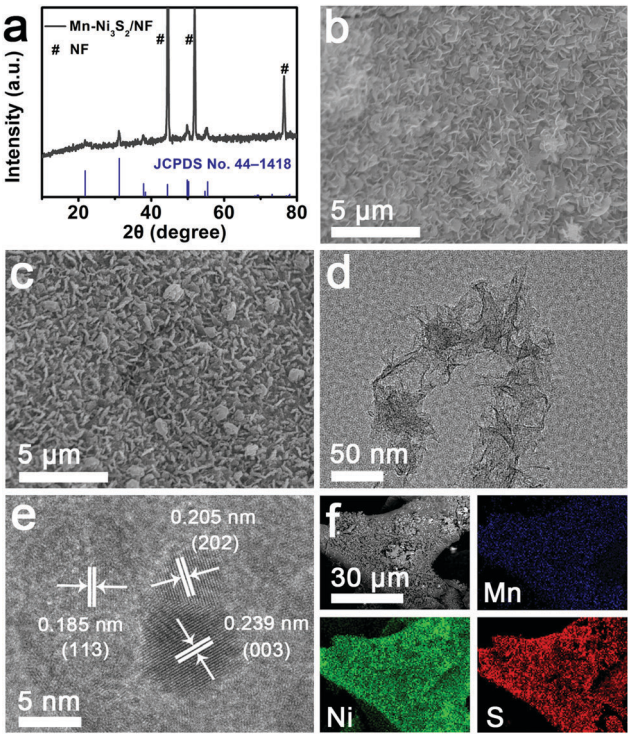

Fig. 1 (a) XRD pattern for Mn-Ni_3S_2/NF. SEM images of (b) hydroxide precursor and (c) Mn-Ni_3S_2/NF. (d) TEM image of Mn-Ni_3S_2 nanosheet. (e) HRTEM image of Mn-Ni_3S_2 nanosheet. (f) EDX elemental mapping images of Mn, Ni and S for Mn-Ni_3S_2/NF.

nanosheet morphology (Fig. 1d). The high-resolution TEM (HRTEM) image shown in Fig. 1e demonstrates the lattice fringe spacings of 0.185, 0.205 and 0.239 nm, which can be ascribed to the (113), (202) and (003) planes of Ni_3S_2. Note that the interplanar distance is slightly longer than that of pure Ni_3S_2 due to the substitution of Mn into Ni_3S_2. The selected area electron diffraction (SAED) pattern (Fig. S3, ESI†) indicates that the three diffraction rings recorded for the Mn-Ni_3S_2 nanosheet can be indexed to the (300), (202) and (003) planes of the Ni_3S_2 phase. As shown in Fig. 1f, energy-dispersive X-ray (EDX) elemental mapping confirms the uniform distribution of Mn, Ni and S elements throughout the whole nanosheet array.

Fig. 2a presents the X-ray photoelectron spectroscopy (XPS) survey spectrum of Mn-Ni_3S_2/NF, further confirming the existence of Mn, Ni and S elements. The Mn $2p_{3/2}$ spectrum (Fig. 2b) shows a peak at 643.6 eV corresponding to Mn^{3+}.[29] The two strong peaks at 855.8 and 873.5 eV can be assigned to the Ni $2p_{3/2}$ and Ni $2p_{1/2}$ states (Fig. 2c), respectively.[30,31] The satellite peaks (identified as "Sat.") at 862.0 and 879.6 eV are the shakeup type peaks of Ni.[32,33] Fig. 2d presents the S 2p region; the peak at 163.1 eV corresponds to S 2p, and the peak at 168.9 eV is assigned to typical Ni–O–S species caused by surface oxidation in air.[34]

The electrocatalytic performance of Mn-Ni_3S_2/NF was evaluated in 1.0 M KOH using a standard three-electrode system with a scan rate of 5 mV s^{-1}. Bare NF, Ni_3S_2/NF, and Pt/C were also tested under the same conditions for comparison. Due to the

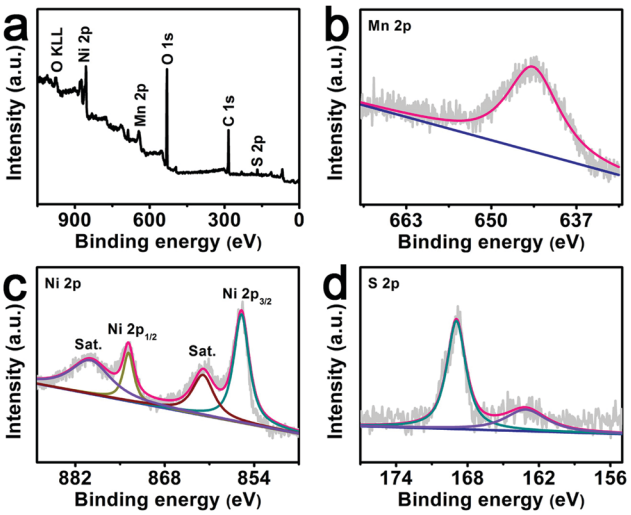

Fig. 2 (a) XPS survey spectrum for Mn-Ni_3S_2/NF. XPS spectra in the (b) Mn 2p, (c) Ni 2p and (d) S 2p regions for Mn-Ni_3S_2/NF.

influence of ohmic resistance, the as-measured reaction currents cannot directly reflect the inherent behavior of the catalysts, therefore an iR compensation was applied to all initial data,[35,36] and all potentials were recorded on a reversible hydrogen electrode (RHE) scale in this work. From the linear sweep voltammetry (LSV) curves (Fig. 3a), we observe that Pt/C shows excellent HER activity and only needs an overpotential of 83 mV to achieve a current density of 10 mA cm^{-2}. Ni_3S_2/NF also shows good catalytic activity with the demand of an overpotential of 198 mV to drive a current density of 10 mA cm^{-2}. As expected, the catalytic performance of Ni_3S_2/NF is significant improved by Mn doping. The overpotential of Mn-Ni_3S_2/NF is 152 mV at the same current density, 46 mV less than that of Ni_3S_2/NF. This performance is better than the performances of Ni_3S_2/AT-NF (200 mV for 10 mA cm^{-2}),[37] MoS_2 (187 mV for 10 mA cm^{-2})[38] and other

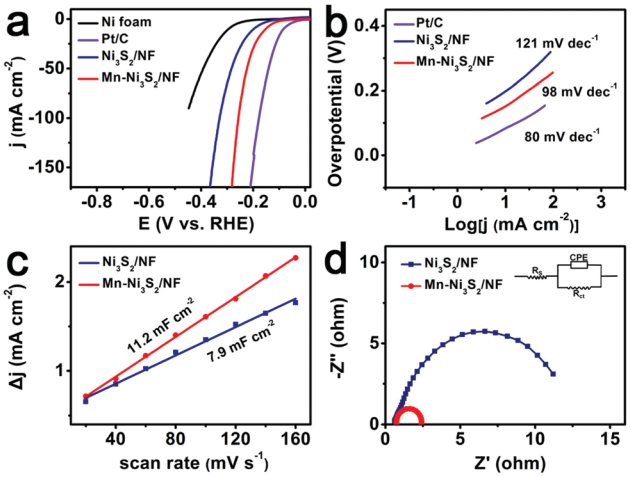

Fig. 3 (a) LSV curves for bare NF, Pt/C, Ni_3S_2/NF and Mn-Ni_3S_2/NF with a scan rate of 5 mV s^{-1}. (b) Tafel plots of Pt/C, Ni_3S_2/NF and Mn-Ni_3S_2/NF. (c) The capacitive currents at 0.36 V as a function of the scan rate for Ni_3S_2/NF and Mn-Ni_3S_2/NF. (d) Nyquist plots of Ni_3S_2/NF and Mn-Ni_3S_2/NF recorded at an overpotential of 200 mV with a fitted equivalent circuit (inset).

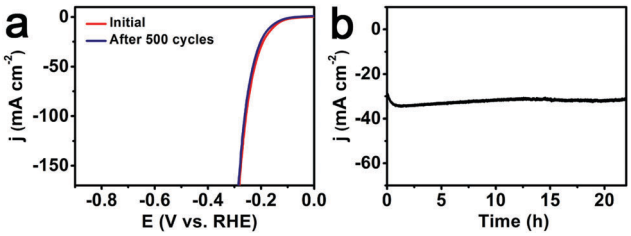

Fig. 4 (a) LSV curves for Mn-Ni_3S_2/NF before and after 500 CV cycles. (b) Time-dependent current density curve of Mn-Ni_3S_2/NF under a static overpotential of 200 mV for at least 20 h.

non-noble metal HER catalysts in alkaline media (Table S1, ESI†). The reaction kinetics of the HER can be estimated by the Tafel equation: $\eta = b \log j + a$, where b is the Tafel slope and j is the current density.[35] As plotted in Fig. 3b, Pt/C shows a Tafel slope of 80 mV dec^{-1}. The Tafel slope of Mn-Ni_3S_2/NF is 98 mV dec^{-1}, lower than that of Ni_3S_2/NF (121 mV dec^{-1}), implying a faster HER kinetics on Mn-Ni_3S_2/NF. Furthermore, we investigated the catalytic performance of Mn-Ni_3S_2/NF with different Mn doping degrees by modulating the atomic ratios of Mn and Ni. As presented in Fig. S4 (ESI†), $Mn_{3\%}$–Ni_3S_2/NF, $Mn_{9\%}$–Ni_3S_2/NF and $Mn_{14\%}$–Ni_3S_2/NF electrodes show decreased HER activity compared with $Mn_{5\%}$–Ni_3S_2/NF, suggesting that the HER activity can be rationally tuned by changing the Mn content.

To reveal the enhanced HER activity of Ni_3S_2/NF after Mn doping, the double layer capacitances (C_{dl}) for Ni_3S_2/NF and Mn-Ni_3S_2/NF were calculated based on cyclic voltammograms (CVs) under different scan rates (Fig. S5, ESI†). As observed in Fig. 3c, we find that the C_{dl} value of Mn-Ni_3S_2/NF (11.2 mF cm^{-2}) is larger than that of Ni_3S_2/NF (7.9 mF cm^{-2}), indicating higher surface roughness and surface area for Mn-Ni_3S_2/NF,[39,40] which is in favor of the enhanced HER activity. The improved electrical conductivity of Mn-Ni_3S_2/NF could be demonstrated *via* electrochemical impedance spectroscopy (EIS) measurements. Nyquist plots show a significant decrease of charge transfer resistance (R_{ct}) from 11.17 Ω for Ni_3S_2/NF to 1.67 Ω for Mn-Ni_3S_2/NF and also a decrease in the series resistance (R_s) from 4.77 Ω to 0.75 Ω (Fig. 3d), suggesting that the HER kinetics on the Mn-Ni_3S_2/NF surface is improved, which is consistent with the analysis of Tafel plots.[41]

Durability is another essential factor to measure the performance of catalysts. As shown in Fig. 4a, Mn-Ni_3S_2/NF only shows a slight loss in the current density after 500 cyclic voltammetry (CV) scans, indicating the superior stability of the catalyst in the electrochemical process. In addition, we also performed the HER at an overpotential of 200 mV, and Mn-Ni_3S_2/NF maintains its catalytic activity for at least 20 h (Fig. 4b). The turnover frequency (TOF) offers an important parameter in evaluating the intrinsic catalytic activity of the catalyst based on the surface site. The number of surface sites was inferred from the electrochemical active surface area (ECSA)[42] (see the ESI† for calculation details). As shown in Fig. S6 (ESI†), Mn-Ni_3S_2/NF achieves a TOF of 0.20 s^{-1} at an overpotential of 200 mV, which is higher than the value of 0.09 s^{-1} obtained from Ni_3S_2/NF at the same overpotential. The above investigations reveal that the enhanced HER activity of Mn-Ni_3S_2/NF can be attributed to the following aspects: (a) the higher surface roughness provides more active sites;[6,19,40] (b) the enhanced electrical conductivity;[41] (c) Mn doping may generate a synergy to optimize electronic environments to improve the intrinsic electric properties of the catalysts.[43,44]

In summary, Mn doping has been experimentally proven as an efficient strategy to enhance the catalytic performance of Ni_3S_2 for alkaline hydrogen evolution. The resulting catalyst exhibits a low overpotential of 152 mV at 10 mA cm^{-2} in 1.0 M KOH. In addition, this catalyst also shows good long-term electrochemical durability with the maintenance of its catalytic activity for at least 20 h. This work not only offers an attractive and cost-effective catalyst for the production of hydrogen under alkaline conditions, but also provides important guidance for designing and synthesizing Ni_3S_2-based catalysts with enhanced HER activity.

This work was supported by the National Natural Science Foundation of China (21775089) and the Outstanding Youth Foundation of Shandong Province (ZR2017JL010).

Conflicts of interest

There are no conflicts to declare.

References

1 M. S. Dresselhaus and I. L. Thomas, *Nature*, 2001, **414**, 332–337.
2 J. Chow, R. J. Kopp and P. R. Portney, *Science*, 2003, **302**, 1528–1531.
3 J. Tian, Q. Liu, A. M. Asiri and X. Sun, *J. Am. Chem. Soc.*, 2014, **136**, 7587–7590.
4 C. Tang, R. Zhang, W. Lu, L. He, X. Jiang, A. M. Asiri and X. Sun, *Adv. Mater.*, 2017, **29**, 1602441.
5 J. Feng, H. Xu, Y. Dong, X. Lu, Y. Tong and G. Li, *Angew. Chem., Int. Ed.*, 2017, **56**, 2960–2964.
6 H. Du, X. Zhang, Q. Tan, R. Kong and F. Qu, *Chem. Commun.*, 2017, **53**, 12012–12015.
7 X. Guo, R. Kong, X. Zhang, H. Du and F. Qu, *ACS Catal.*, 2018, **8**, 651–655.
8 M. G. Walter, E. L. Warren, J. R. McKone, S. W. Boettcher, Q. Mi, E. A. Santori and N. S. Lewis, *Chem. Rev.*, 2010, **110**, 6446–6473.
9 A. Sivanantham, P. Ganesan and S. Shanmugam, *Adv. Funct. Mater.*, 2016, **26**, 4661–4672.
10 H. T. Bui, N. K. Shrestha, S. Khadtare, C. D. Bathula, L. Giebeler, Y. Y. Noh and S. H. Han, *ACS Appl. Mater. Interfaces*, 2017, **9**, 18015–18021.
11 M. Gong, W. Zhou, M. Tsai, J. Zhou, M. Guan, M. Lin, B. Zhang, Y. Hu, D. Wang, J. Yang, S. J. Pennycook, B. Hwang and H. Dai, *Nat. Commun.*, 2014, **5**, 4695.
12 C. Tang, N. Cheng, Z. Pu, W. Xing and X. Sun, *Angew. Chem., Int. Ed.*, 2015, **54**, 9351–9355.
13 T. Li, K. Niu, M. Yang, N. K. Shrestha, Z. Gao and Y. Y. Song, *J. Power Sources*, 2017, **356**, 89–96.
14 D. V. Shinde, S. A. Patil, K. Cho, D. Y. Ahn, N. K. Shrestha, R. S. Mane, J. K. Lee and S. H. Han, *Adv. Funct. Mater.*, 2015, **25**, 5739–5747.
15 Q. Ma, C. Hu, K. Liu, S. Hung, D. Ou, H. Chen, G. Fu and N. Zheng, *Nano Energy*, 2017, **41**, 148–153.
16 L. Feng, G. Yu, Y. Wu, G. D. Li, H. Li, Y. Sun and X. Zou, *J. Am. Chem. Soc.*, 2015, **137**, 14023–14026.
17 C. Yang, M. Gao, Q. Zhang, J. Zeng, X. Li and A. P. Abbott, *Nano Energy*, 2017, **36**, 85–94.
18 Y. Wu, G. Li, Y. Liu, L. Yang, X. Lian, T. Asefa and X. Zou, *Adv. Funct. Mater.*, 2016, **26**, 4839–4847.
19 T. Liu, D. Liu, F. Qu, D. Wang, L. Zhang, R. Ge, S. Hao, Y. Ma, G. Du, A. M. Asiri, L. Chen and X. Sun, *Adv. Energy Mater.*, 2017, **7**, 1700020.
20 H. Du, L. Xia, S. Zhu, F. Qu and F. Qu, *Chem. Commun.*, 2018, **54**, 2894–2897.

21 D. Wang, M. Gong, H. Chou, C. Pan, H. Chen, Y. Wu, M. Lin, M. Guan, J. Yang, C. Chen, Y. Wang, B. Hwang, C. Chen and H. Dai, *J. Am. Chem. Soc.*, 2015, **137**, 1587–1592.
22 T. Liu, A. M. Asiri and X. Sun, *Nanoscale*, 2016, **8**, 3911–3915.
23 R. Zhang, C. Tang, R. Kong, G. Du, A. M. Asiri, L. Chen and X. Sun, *Nanoscale*, 2017, **9**, 4793–4800.
24 P. Wang, Z. Pu, Y. Li, L. Wu, Z. Tu, M. Jiang, Z. Kou and I. S. Amiinu, *ACS Appl. Mater. Interfaces*, 2017, **9**, 26001–26007.
25 B. M. Hunter, H. B. Gray and A. M. Muller, *Chem. Rev.*, 2016, **116**, 14120–14136.
26 Y. Meng, W. Song, H. Huang, Z. Ren, S. Chen and S. L. Suib, *J. Am. Chem. Soc.*, 2014, **136**, 11452–11464.
27 Y. Feng, Y. OuYang, L. Peng, H. Qiu, H. Wang and Y. Wang, *J. Mater. Chem. A*, 2015, **3**, 9587–9594.
28 G. Zhang, Y. Feng, W. Lu, D. He, C. Wang, Y. Li, X. Wang and F. Cao, *ACS Catal.*, 2018, **8**, 5431–5441.
29 M. B. Zakaria, C. Li, M. Pramanik, Y. Tsujimoto, M. Hu, V. Malgras, S. Tominaka and Y. Yamauchi, *J. Mater. Chem. A*, 2016, **4**, 9266–9274.
30 W. Zhou, X. Wu, X. Cao, X. Huang, C. Tian, J. Tian, H. Liu, J. Wang and H. Zhang, *Energy Environ. Sci.*, 2013, **6**, 2921–2924.
31 B. Zhang, X. Ye, W. Dai, W. Hou and Y. Xie, *Chem. – Eur. J.*, 2006, **12**, 2337–2342.
32 M. C. Biesinger, B. P. Payne, L. W. M. Lau, A. Gerson and R. S. C. Smart, *Surf. Interface Anal.*, 2009, **41**, 324–332.
33 X. Liu, J. Liu and X. Sun, *J. Mater. Chem. A*, 2015, **3**, 13900–13905.
34 C. Dueso, M. T. Izquierdo, F. García-Labiano, F. Luis, A. Abad, P. Gayán and J. Adánez, *Appl. Catal., B*, 2012, **126**, 186–199.
35 Z. Xing, Q. Liu, A. M. Asiri and X. Sun, *Adv. Mater.*, 2014, **26**, 5702–5707.
36 X. Zhang, S. Zhu, L. Xia, C. Si, F. Qu and F. Qu, *Chem. Commun.*, 2018, **54**, 1201–1204.
37 C. Ouyang, X. Wang, C. Wang, X. Zhang, J. Wu, Z. Ma, S. Dou and S. Wang, *Electrochim. Acta*, 2015, **174**, 297–301.
38 M. A. Lukowski, A. S. Daniel, F. Meng, A. Forticaux, L. Li and S. Jin, *J. Am. Chem. Soc.*, 2013, **135**, 10274–10277.
39 X. Zhang, C. Si, X. Guo, R. Kong and F. Qu, *J. Mater. Chem. A*, 2017, **5**, 17211–17215.
40 T. Kou, T. Smart, B. Yao, I. Chen, D. Thota, Y. Ping and Y. Li, *Adv. Energy Mater.*, 2018, 1703538.
41 Y. Li, H. Zhang, M. Jiang, Y. Kuang, X. Sun and X. Duan, *Nano Res.*, 2016, **9**, 2251–2259.
42 J. Kibsgaard, C. Tsai, K. Chan, J. D. Benck, J. K. Nørskov, F. AbildPedersen and T. F. Jaramillo, *Energy Environ. Sci.*, 2015, **8**, 3022–3029.
43 Y. Zhu, C. Su, X. Xu, W. Zhou, R. Ran and Z. Shao, *Chem. – Eur. J.*, 2014, **20**, 15533–15542.
44 X. Long, G. Li, Z. Wang, H. Zhu, T. Zhang, S. Xiao, W. Guo and S. Yang, *J. Am. Chem. Soc.*, 2015, **137**, 11900–11903.